Structure of amorphous $GeSe_9$ by neutron diffraction and first-principles molecular dynamics: Impact of trajectory sampling and size effects

Sébastien Le Roux,[1] Assil Bouzid,[2] Kye Yeop Kim,[3] Seungwu Han,[3] Anita Zeidler,[4] Philip S. Salmon,[4] and Carlo Massobrio[1]

[1]*Institut de Physique et de Chimie des Matériaux de Strasbourg, 23 rue du Loess, BP 43, F-67034 Strasbourg Cedex 2, France*

[2]*Chaire de Simulation à l'Echelle Atomique (CSEA), Ecole Polytechnique Fédérale de Lausanne (EPFL), CH-1015 Lausanne, Switzerland*

[3]*Department of Materials Science and Engineering, Seoul National University, Seoul 151-744, Korea*

[4]*Department of Physics, University of Bath, Bath BA2 7AY, United Kingdom*

(Dated: July 29, 2016)

The structure of glassy $GeSe_9$ was investigated by combining neutron diffraction with density-functional-theory-based first-principles molecular dynamics. In the simulations, three different models of $N = 260$ atoms were prepared by sampling three independent temporal trajectories, and the glass structures were found to be substantially different from those obtained for models in which smaller numbers of atoms or more rapid quench rates were employed. In particular, the overall network structure is based on Se_n chains that are cross-linked by $Ge(Se_4)_{1/2}$ tetrahedra, where the latter are predominantly corner as opposed to edge sharing. The occurrence of a substantial proportion of Ge-Se-Se connections does not support a model in which the material is phase separated into Se-rich and $GeSe_2$-rich domains. The appearance of a first-sharp diffraction peak in the Bhatia-Thornton concentration-concentration partial structure factor does, however, indicate a non-uniform distribution of the Ge-centered structural motifs on an intermediate length scale.

PACS numbers: 61.43.Fs, 71.15.Pd, 61.05.F-
Keywords: Glass structure, chalcogenide glass, first-principles molecular dynamics, neutron diffraction

I. INTRODUCTION

Glassy Se is the archetypal 1-dimensional elemental amorphous solid, in which the Se atoms bind to form extended Se_n chains (n is an integer ≥ 2).[1] The introduction of Ge leads to the formation of cross-links between the Se_n chains that increase the network dimensionality, and the ability of Ge and Se to adopt a rich variety of structural motifs ensures that the Ge_xSe_{1-x} system has a large glass-forming region ($0 \leq x \leq 0.43$).[2] The Ge-Se system is therefore a prototype for investigating the topology of disordered networks,[3–24] and has featured prominently in the development of mean-field constraint-counting theory for network glasses,[25,26] and in the identification and characterization of the so-called intermediate phase for this class of materials.[27–29]

The similarity between the electronegativity values of Ge and Se favors the use of first-principles molecular dynamics (FPMD) to produce atomistic models that are in quantitative agreement with experiment.[30–35] There are, however, questions related to the system size and the protocol that is used to prepare a glass from the liquid state. In the case of glassy $GeSe_9$, for example, two different sets of FPMD simulations have been performed, and the results have been compared to those obtained from neutron diffraction. In the first, Tafen and Drabold[36] employed a periodic cell with $N = 400$ atoms (i.e., 40 Ge atoms) and a rapid quench-rate (the system temperature was decreased from $T = 2200$ K to $T = 300$ K in 5 ps) to obtain a disordered structure that contained large fractions of both one-fold coordinated ($\simeq$19.6%) and three-fold coordinated ($\simeq$20.4%) Se atoms. In view of the results found for glassy $GeSe_4$ by using FPMD with a slower quench-rate and longer room-temperature relaxation time,[33,37,38] the presence of such a large fraction of mis-coordinated Se atoms may originate from a structure that was insufficiently annealed on cooling, i.e., the solid retained too much memory of the highly-diffusive liquid-state. In the second, Micoulaut et al.[22] addressed this issue by exploiting much longer temporal trajectories, especially at room temperature (84 ps). The periodic cell size used in this work was, however, small at $N = 120$ (i.e., 12 Ge atoms), and the Se_n chains were found to be interconnected by a surprisingly large number of edge-sharing Ge-centered tetrahedra, where the ratio of edge sharing (ES) to corner sharing (CS) $Ge(Se_4)_{1/2}$ tetrahedra ES/CS = 0.86. Thus, there is uncertainty regarding the best way of modeling the glass structure when Ge is first added to Se.

We have therefore been motivated to reconsider the atomic structure of glassy $GeSe_9$ by performing (i) a neutron diffraction experiment to investigate the reliability of previous experimental work,[39] and (ii) FPMD simulations with a large system size ($N = 260$) and variety of quench-scheme and relaxation protocols, with the intent of improving the reliability of the atomic-scale simulation approach. The models were obtained by sampling three independent temporal trajectories and are consistent with the new neutron diffraction results. They show that the Se atoms are predominantly two-fold coordinated, i.e., there is a negligible fraction of mis-coordinated Se atoms, and give an ES to CS ratio of $Ge(Se_4)_{1/2}$ tetrahedra that is appreciably smaller than found in Ref. 22, in keeping with the expectation from experiment.[18,40]

The paper is organized as follows. The experimental methods are described in Sec. II, where the glass preparation protocol is given in some detail in order to allow for sample reproducibility, and in case there are differences in structure that result from different preparation methods. The FPMD methods are described in Sec. III. The results for glassy $GeSe_9$ in both reciprocal space and real space are then presented and discussed in Secs. IV and V, respectively. The simulation protocols are discussed in Sec. VI. Conclusions are drawn in

Sec. VII.

II. NEUTRON DIFFRACTION EXPERIMENTS

A glassy $GeSe_9$ sample was prepared by loading elemental Ge and Se powders (99.999 %, Sigma-Aldrich), with the correct mass ratio, into a silica ampoule of 5 mm inner diameter and 1 mm wall thickness that had been etched using a 48 wt% solution of hydrofluoric acid, rinsed using water then acetone, and baked dry under vacuum at 1073 K for 3 h. The ampoule was loaded in a high-purity argon-filled glove box, isolated using a Young's tap, and then transferred to a vacuum line where it was sealed under a pressure of 10^{-5} Torr. The sealed ampoule was placed in a rocking furnace, which was heated at a rate of 2 K min^{-1} from ambient to a temperature T = 1248 K, dwelling for 1 h each at T = 494 K, T = 958 K and T = 1211 K, near to the melting and boiling points of Se, and the melting point of Ge, respectively. The highest temperature was maintained for 47 h before the rocking motion was stopped, the furnace was placed vertically for 1 h to let the melt collect at the bottom of the ampoule, the furnace was cooled at a rate of 2 K min^{-1} to T = 594 K where the sample was left to equilibrate for 4 h, and the ampoule was then dropped into an ice/water mixture. The sample was broken out of the ampoule inside an argon-filled glove box and transferred into a vanadium container of outer diameter 7 mm and wall thickness 0.1 mm ready for the diffraction experiment.

The neutron diffraction experiment was performed using the GEM diffractometer[41] at the ISIS pulsed neutron source. Diffraction patterns were measured for the $GeSe_9$ sample in its vanadium container, the empty container, the empty instrument, and a vanadium rod of diameter 8.37(1) mm for normalization purposes. Each diffraction pattern was built up from the intensities measured for different detector groups, where the intensities were saved at regular intervals in order to verify the stability of the diffractometer.[42] The data sets were analyzed detector by detector using the GUDRUN analysis software.[43] The atomic number density of the glass ρ = 0.0333(1) $Å^{-3}$, as measured using a Quantachrome MICROULTRAPYC 1200*e* pycnometer operated with helium gas. The glass transition temperature was measured to be T_g(onset) = 365(6) K or T_g(midpoint) = 372(4) K by using modulated differential scanning calorimetry with a scan rate of 3 K min^{-1} and modulation of 1 K per 100 s.

III. FIRST-PRINCIPLES MOLECULAR DYNAMICS SIMULATIONS

The simulations were performed at constant volume on a system containing $N = 260$ atoms (26 Ge and 234 Se). A periodically repeated cubic cell of size-length L = 19.9 Å was used, corresponding to the experimental density of the glass at $T = 300$ K. This strategy was chosen because it is less time consuming and more tractable than attempting to track the liquid-state quench through the implementation of a set of constant pressure simulations at variable density, where large error bars are associated with each calculated pressure. The system size ensures that the minimum magnitude of the scattering vector $k_{min} = 0.3157$ $Å^{-1}$ is significantly smaller than the position of the first-sharp diffraction peak (FSDP) at $k_{FSDP} \simeq 1$ $Å^{-1}$ for Ge_xSe_{1-x} glasses, a feature that appears because of ordering on an intermediate length scale.[13] The electronic structure was described within density functional theory (DFT) and evolved self-consistently during the motion.[44] We employed the generalized gradient approximation after Becke (B) for the exchange energy and Lee, Yang and Parr (LYP) for the correlation energy.[45,46] The reasons underpinning this choice of the exchange-correlation functional are described in recent work on liquid and glassy $GeSe_2$, where the structures obtained from the BLYP and Perdew and Wang (PW) functionals are compared.[47–49] In short, the BLYP approach gives a better description of the short-range structure, especially for the local environment of Ge, because it gives a better account of valence-electron localization effects. The valence electrons were treated explicitly, in conjunction with norm-conserving pseudo-potentials of the Trouiller-Martins type to account for core-valence interactions.[50] The wave functions were expanded at the Γ point of the supercell using a plane-wave basis-set with an energy cutoff $E_{cut} = 30$ Ry. The simulations were implemented using a fictitious electron mass of 1000 a.u. (i.e., in units of $m_e a_0^2$ where m_e is the electron mass and a_0 is the Bohr radius) and a time step of $\Delta t = 0.24$ fs to integrate the equations of motion. A fictitious electron mass of 1000 a.u. ensures the best compromise between small departures from the Born-Oppenheimer surface, which are reduced by decreasing the fictitious mass, and the value of the time step, which can become unaffordably small for a vanishing small fictitious mass.

The liquid at T = 1000 K, fully equilibrated for a period of 10 ps, was used as a starting point to prepare three different models for the glassy material with contrasting thermal histories. In the following, these models will be referred to as II–IV (model I will refer to the FPMD results taken from Ref. 22). Here, the selection of the starting configuration density to be that of the glass is legitimate, provided the molecular dynamics trajectories are truly liquid-like, i.e., they have a highly diffusive character. This is indeed the case for our FPMD simulations of liquid $GeSe_9$ where the diffusion coefficients are greater than 1×10^{-5} cm^2 s^{-1}. In view of the variation in glass structure that results from different simulation protocols (see below), the difference between the uppermost simulated (T = 1000 K) and experimental (T = 1248 K) liquid-state temperatures is not expected to be significant. Model II was obtained via a two-step schedule with annealing times of $\simeq$5 ps at T = 600 K and $\simeq$5 ps at T = 300 K. Model III was obtained via a two-step schedule with annealing times of $\simeq$8 ps at T = 600 K and $\simeq$8 ps at T = 300 K. Model IV was obtained via a three-step schedule with annealing times of $\simeq$12.5 ps at T = 900 K, $\simeq$25 ps at T = 600 K and $\simeq$30 ps at T = 300 K. Hence, the overall rate of reduction in the temperature is roughly 7×10^{13} K s^{-1}, 4.375×10^{13} K s^{-1} and 1.04×10^{13} K s^{-1} for models II to IV, respectively. At the end of these procedures, the glasses for models II and IV were relaxed for $\simeq$30 ps at T = 300 K and configurations were saved

after every 10 ps step, whereas the glass for model III was relaxed for a much shorter time of ≃5 ps at T = 300 K.

These modeling protocols were chosen in order to explore the impact on the glass structure of (i) the quench-rate schedule and (ii) the time spent on relaxing the glass structure at the target temperature. For example, the quench temperatures of T = 600 K and T = 300 K for models II and III were the same and the annealing times at these temperatures were similar (5–8 ps), but model II was subsequently relaxed for much longer (30 ps) at room temperature. In comparison, an additional quench temperature was used for model IV along with longer annealing times (12.5–30 ps), and this model was subsequently relaxed for a long time (30 ps) at room temperature. Thus, models II and III will give insight into the affect on the glass structure of an extended relaxation time at room temperature, whereas models II and IV will give insight into the affect on the glass structure of a more extended procedure for quenching from the melt.

IV. RECIPROCAL-SPACE PROPERTIES

A. Total structure factor

In a neutron diffraction experiment on a Ge-Se glass, the measured total structure factor is given by[51]

$$S_{\rm T}(k) = 1 + \sum_{\alpha}\sum_{\beta} \frac{c_\alpha c_\beta b_\alpha b_\beta}{\langle b\rangle^2}\left[S^{\rm FZ}_{\alpha\beta}(k) - 1\right] \qquad (1)$$

where α and β denote the chemical species (Ge or Se), c_α and b_α represent the atomic fraction and coherent neutron scattering length of chemical species α, respectively, $\langle b\rangle = c_{\rm Ge}b_{\rm Ge} + c_{\rm Se}b_{\rm Se}$ is the mean scattering length, $S^{\rm FZ}_{\alpha\beta}(k)$ is a so-called Faber-Ziman (FZ) partial structure factor, and k is the magnitude of the scattering vector. For a sample of glassy $GeSe_9$ containing Ge and Se of natural isotopic abundance, the coherent neutron scattering lengths are $b_{\rm Ge}$ = 8.185(20) fm and $b_{\rm Se}$ = 7.970(9) fm,[52] such that the relative weighting factors for the Ge-Ge, Ge-Se and Se-Se $S^{\rm FZ}_{\alpha\beta}(k)$ functions are 0.0105: 0.1839: 0.8056. In consequence, $S_{\rm T}(k)$ is dominated by $S^{\rm FZ}_{\rm SeSe}(k)$. Also, the similarity between the values of $b_{\rm Ge}$ and $b_{\rm Se}$ ensures that $S_{\rm T}(k) \simeq S_{\rm NN}(k)$ to an excellent level of approximation,[13] where $S_{\rm NN}(k)$ is the Bhatia-Thornton[53] number-number partial structure factor and describes the topological ordering of the glass.[54]

The $S_{\rm T}(k)$ function measured in the present work is shown in Fig. 1. Its reliability was assessed by performing the usual self-consistency checks,[55] e.g., (i) it satisfies the sum-rule relation $\int_0^\infty {\rm d}k\, k^2\,[S_{\rm T}(k) - 1] = -2\pi^2\rho$; (ii) the corresponding total pair-distribution function $g_{\rm T}(r)$ (Sec. V A) oscillates about zero at r-values smaller than the distance of closest approach between two atoms; and (iii) when these low-r oscillations are set to zero, the back Fourier transform of $g_{\rm T}(r)$ is in good overall agreement with the original $S_{\rm T}(k)$ function. As shown in Fig. 1, the newly measured $S_{\rm T}(k)$ function is different to that obtained in the neutron diffraction work of Ramesh Rao et al.[39] Both data sets show a shoulder at $k \simeq 1.3$ Å^{-1}, i.e., in the region of the FSDP expected for Ge-Se glasses,[13] but there is otherwise a large discrepancy in the low-k region. The latter may originate from a background scattering issue in the earlier neutron diffraction work. In Fig. 1, the experimental results are also compared to the $S_{\rm T}(k)$ functions from FPMD models I–IV, where model I originates from Ref. 22 and models II–IV originate from the present work (Sec. III). The latter are in good overall agreement with the $S_{\rm T}(k)$ function measured in the present work, including the low-k region.

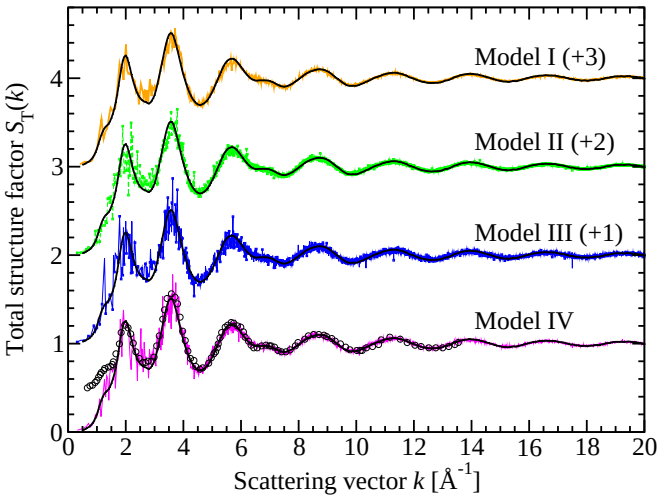

Figure 1: (Color online) The neutron total structure factor $S_{\rm T}(k)$ for glassy $GeSe_9$. The measured $S_{\rm T}(k)$ function from the present work is given by the solid (black) curves with vertical error bars, where the size of the error bars is smaller than the line thickness at most k values, and the measured $S_{\rm T}(k)$ function from Ref. 39 is given by the (black) circles. The experimental results are compared to those obtained from FPMD models I (solid orange curve),[22] II (broken green curve with squares), III (solid blue curve with squares) and IV (solid magenta curve) by a direct calculation in reciprocal space. Several of the data sets have been shifted vertically for clarity of presentation.

B. Partial structure factors

The partial structure factors for glassy $GeSe_9$ from models I–IV are shown in Fig. 2. The profile of a given $S^{\rm FZ}_{\alpha\beta}(k)$ function is similar for each of the models, and as expected from the glass composition, $S^{\rm FZ}_{\rm SeSe}(k)$ follows very closely the profile of $S_{\rm T}(k)$. An FSDP is observable in both $S^{\rm FZ}_{\rm GeGe}(k)$ and $S^{\rm FZ}_{\rm GeSe}(k)$ at $k_{\rm FSDP} \simeq 1.02$–1.07 Å^{-1} and $k_{\rm FSDP} \simeq 1.17$–1.29 Å^{-1}, respectively, where the height of this peak is larger for $S^{\rm FZ}_{\rm GeGe}(k)$ as compared to $S^{\rm FZ}_{\rm GeSe}(k)$ and does not change markedly between the models. Thus, there is ordering on an intermediate length scale that is associated with the Ge-β (β = Ge or Se) correlations, but not with the Se-Se correlations. The nature of this ordering can be explored further by constructing the Bhatia-Thornton[53] concentration-concentration partial structure factor

$$S_{\rm CC}(k) = c_{\rm Ge}c_{\rm Se}\{1 + c_{\rm Ge}c_{\rm Se}\left[S^{\rm FZ}_{\rm GeGe}(k) + S^{\rm FZ}_{\rm SeSe}(k) - 2S^{\rm FZ}_{\rm GeSe}(k)\right]\}, \qquad (2)$$

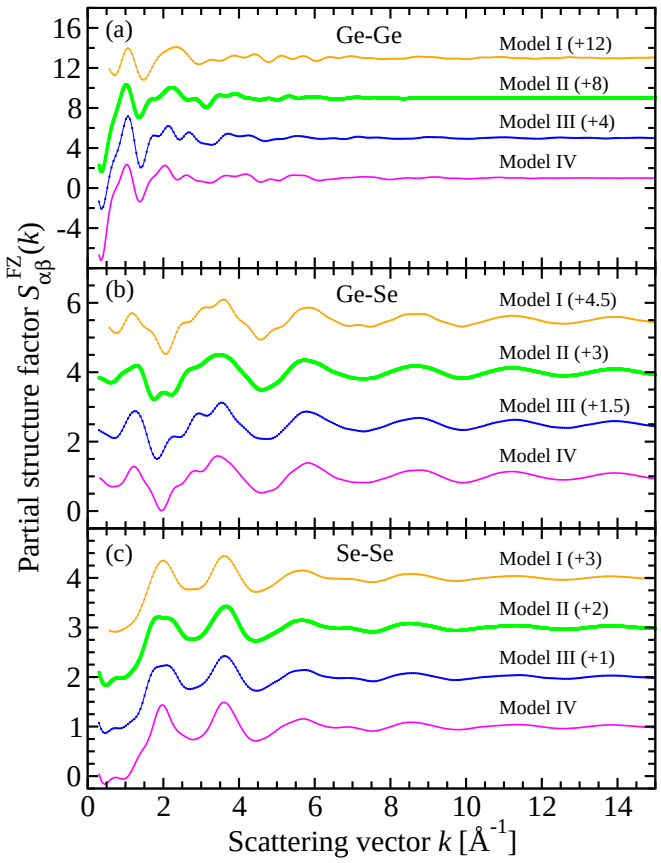

Figure 2: (Color online) The (a) Ge-Ge, (b) Ge-Se and (c) Se-Se Faber-Ziman partial structure factors $S^{FZ}_{\alpha\beta}(k)$ for glassy $GeSe_9$ from FPMD models I (solid orange curve),[22] II (broken green curve with squares), III (solid blue curve with squares) and IV (solid magenta curve). The functions were obtained by Fourier transforming the $g_{\alpha\beta}(r)$ functions shown in Fig. 5. Several of the data sets have been shifted vertically for clarity of presentation.

which can be approximated to

$$S_{CC}(k) \simeq c_{Ge}c_{Se}\left\{1 + c_{Ge}c_{Se}\left[S^{FZ}_{GeGe}(k) - 2S^{FZ}_{GeSe}(k)\right]\right\} \quad (3)$$

in the region of the FSDP because of an absence of this feature in $S_{SeSe}(k)$. The appearance of an FSDP in $S_{CC}(k)$ for each of the FPMD models (Fig. 3) indicates the presence of concentration fluctuations on an intermediate length scale that are associated with the Ge-β correlation functions.[6,54] In particular, the FSDP will be associated with a distribution of Ge-centered motifs having a periodicity of $2\pi/k_{FSDP}$ and correlation length of $2\pi/\Delta k_{FSDP}$, where Δk_{FSDP} is the full-width at half-maximum of the FSDP,[56] i.e., the Ge atoms will not be uniformly distributed on an intermediate length scale. In systems such as liquid $GeSe_2$, the presence of an FSDP in $S_{CC}(k)$ is related to the four-fold rings formed by ES $Ge(Se_4)_{1/2}$ tetrahedra.[57] These motifs lead to regions where the Ge atoms are more clustered as compared to a homogenous distribution of CS $Ge(Se_4)_{1/2}$ linkages, leading to a periodic distribution of Ge atoms with a finite correlation length. As will be discussed in Sec. V B, the ratio ES/CS = 0.08–0.18 in models

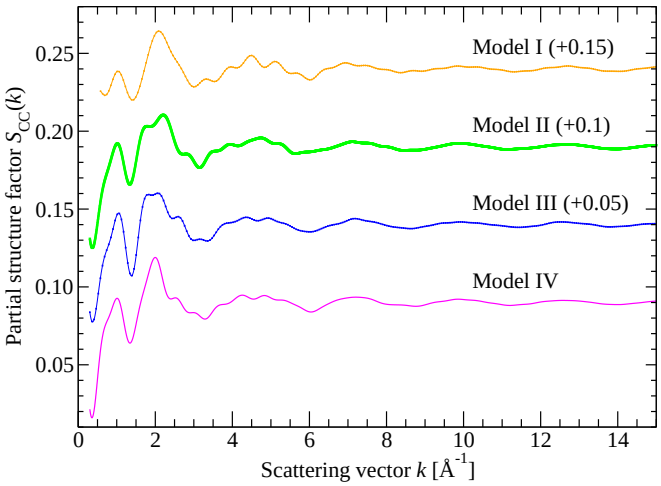

Figure 3: (Color online) The Bhatia-Thornton concentration-concentration partial structure factor $S_{CC}(k)$ for glassy $GeSe_9$ from FPMD models I (solid orange curve),[22] II (broken green curve with squares), III (solid blue curve with squares) and IV (solid magenta curve). Several of the data sets have been shifted vertically for clarity of presentation.

II–IV for glassy $GeSe_9$. It is worthwhile noting that the width of the FSDP is similar for both the $N = 120$ and $N = 260$ systems, i.e., the correlation length for the Ge-centered motifs does not appear to show a clear dependence on the system size. This observation is in line with the results obtained previously for the behavior of the FSDP in liquid $GeSe_2$, where it was shown by Fourier transformation that the essential features of the FSDP can be captured provided the cutoff of the integration range for the real-space pair-correlation functions is in the range 6–10.5 Å.[58] Here, the upper-limit is smaller than $\sqrt{2}L/2$, a value for which reliable statistics can be gathered for distances between independent atoms in a cubic supercell of side-length L for a system of $N = 120$ atoms.

V. REAL-SPACE PROPERTIES

A. Total pair-distribution function

The neutron total pair-distribution function is given by the Fourier transform relation

$$g_T(r) = 1 + \frac{1}{2\pi^2\rho r}\int_0^\infty dk\, k\,[S_T(k) - 1]\sin(kr) \quad (4)$$
$$= \sum_\alpha\sum_\beta \frac{c_\alpha c_\beta b_\alpha b_\beta}{\langle b\rangle^2}\left[g_{\alpha\beta}(r) - 1\right]$$

where $g_{\alpha\beta}(r)$ is a partial pair-distribution function. In the case of glassy $GeSe_9$, the small concentration of Ge means that $g_T(r)$ will be dominated by $g_{SeSe}(r)$, so that $g_T(r)$ will be largely insensitive to the detail in $g_{GeGe}(r)$. In Fig. 4, the $g_T(r)$ function obtained by Fourier transforming the measured $S_T(k)$ function of the present work is compared to the calculated $g_T(r)$ function for models I–IV, as obtained by combin-

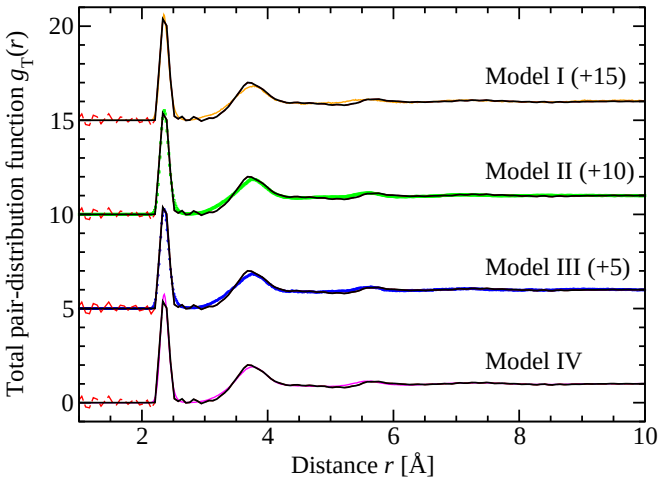

Figure 4: (Color online) The neutron total pair-distribution function $g_T(r)$ for glassy $GeSe_9$. The measured $g_T(r)$ function from the present work [solid (black) curves] was obtained by Fourier transforming the spline-fitted measured $S_T(k)$ function shown in Fig. 1 with k_{max} = 30 Å^{-1}. The Fourier transform artifacts at r values smaller than the distance of closest approach between two atoms are shown by the chained (red) curves. The experimental results are compared to those obtained from FPMD models I (solid orange curve),[22] II (broken green curve with squares), III (solid blue curve with squares) and IV (solid magenta curve). Several of the data sets have been shifted vertically for clarity of presentation.

ing the $g_{\alpha\beta}(r)$ functions shown in Fig. 5. All of the models give a good account of this measured $g_T(r)$ function because (i) $g_{SeSe}(r)$ receives the predominant weighting in the expression for $g_T(r)$ (Eq. (4)) and (ii) all of the calculated $g_{SeSe}(r)$ functions have very similar profiles.

The similarity between the coherent neutron scattering lengths of Ge and Se of natural isotopic abundance (Sec. IV A) ensures that $g_T(r) \simeq g_{NN}(r)$ to an excellent level of approximation,[13] where $g_{NN}(r)$ is the Bhatia-Thornton[53] number-number partial pair-distribution function

$$g_{NN}(r) \equiv c_{Ge}^2 g_{GeGe}(r) + c_{Se}^2 g_{SeSe}(r) + 2c_{Ge}c_{Se}g_{GeSe}(r). \quad (5)$$

It follows that the overall mean coordination number $\bar{n}$ is given by

$$\begin{aligned} \bar{n} &= 4\pi\rho \int_{r_i}^{r_j} dr\, r^2 g_{NN}(r) \\ &= c_{Ge}\bar{n}_{Ge} + c_{Se}\bar{n}_{Se} \end{aligned} \quad (6)$$

where $\bar{n}_{Ge} = \bar{n}_{GeGe} + \bar{n}_{GeSe}$ and $\bar{n}_{Se} = \bar{n}_{SeSe} + \bar{n}_{SeGe}$ are the mean Ge and Se coordination numbers, respectively, $\bar{n}_{\alpha\beta}$ denotes the mean coordination number of atoms of type β, contained in a volume defined by two concentric spheres of radii r_i and r_j centered on an atom of type α, and $\bar{n}_{SeGe} / c_{Ge} = \bar{n}_{GeSe} / c_{Se}$. Table I shows that the value of $\bar{n}$ = 2.20(1) obtained from the present neutron diffraction work is in agreement with that expected from the '8-N' rule, which predicts that $\bar{n}_{Ge}$ = 4 and $\bar{n}_{Se}$ = 2 such that $\bar{n}$('8-N') = 2.2. This value is smaller than the value of $\bar{n}$ = 2.45(18) obtained in the previous neutron diffraction work of Ramesh Rao et al.[39]

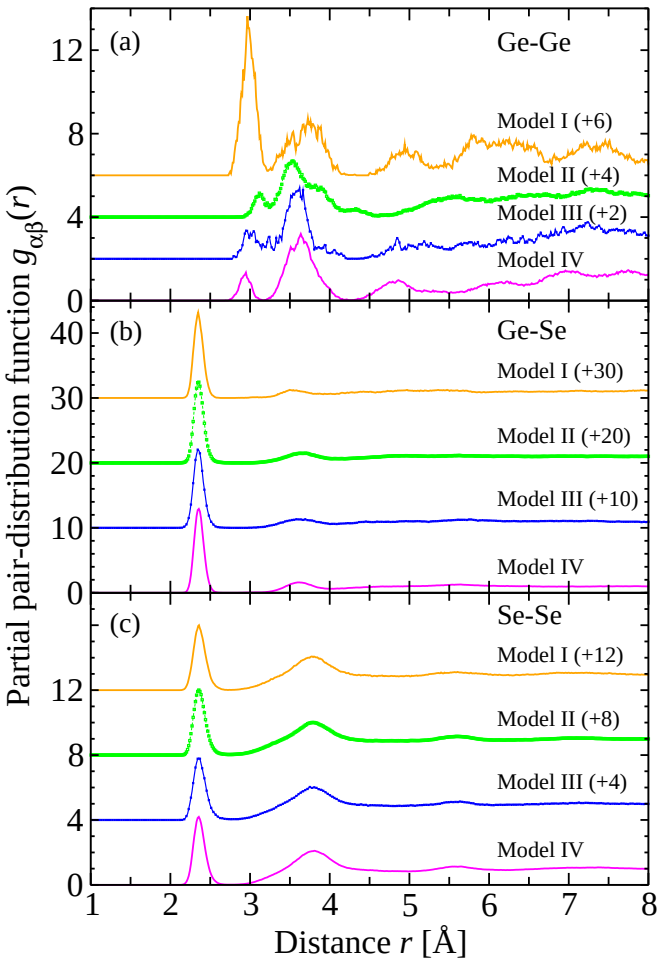

Figure 5: (Color online) The (a) Ge-Ge, (b) Ge-Se and (c) Se-Se partial pair-distribution functions $g_{\alpha\beta}(r)$ for glassy $GeSe_9$ from FPMD models I (solid orange curve),[22] II (broken green curve with squares), III (solid blue curve with squares) and IV (solid magenta curve). Several of the data sets have been shifted vertically for clarity of presentation.

Table I: The mean Ge and Se coordination numbers $\bar{n}_{Ge}$ and $\bar{n}_{Se}$ for glassy $GeSe_9$, as measured by using neutron diffraction (ND) or calculated by using FPMD with a cutoff distance r_{cut} = 2.75 Å. The overall mean coordination number, $\bar{n}$, is also listed, and is compared to the value expected from the '8-N' rule.

Source	$\bar{n}_{Ge}$	$\bar{n}_{Se}$	$\bar{n}$	$\bar{n}$('8-N')
ND (present work)	–	–	2.20(1)	2.2
ND (Ref. 39)	4.0	1.8(2)	2.45(18)	2.2
Models I (Ref. 22) – IV	4.0	2.0	2.2	2.2

B. Partial pair-distribution functions

The partial pair-distribution functions for models I–IV are shown in Fig. 5, and the associated coordination numbers $\bar{n}_{\alpha\beta}$ are listed in Table II, where the integration range was set to

Table II: The coordination numbers $\bar{n}_{\alpha\beta}$ obtained from the FPMD models by using an integration range of 0–2.75 Å, where the upper limit corresponds to the minimum after the first peak in $g_T(r)$. The predictions of the CON and RCN models are also listed.[13]

Model	$\bar{n}_{GeGe}$	$\bar{n}_{GeSe}$	$\bar{n}_{SeGe}$	$\bar{n}_{SeSe}$
I (Ref. 22)	0.0	4.0	0.44	1.56
II – IV	0.0	4.0	0.44	1.56
CON	0.0	4.0	0.44	1.56
RCN	0.73	3.27	0.36	1.63

include distances up to the first minimum in $g_T(r)$. The values for $\bar{n}_{Ge}$ and $\bar{n}_{Se}$ are listed in Table I, along with the overall mean coordination number $\bar{n}$.

In the case of $g_{SeSe}(r)$, the first peak at $\simeq$2.36 Å originates from Se-Se homopolar bonds, and gives a coordination number $\bar{n}_{SeSe}$ = 1.56 that is insensitive to the model. In the case of $g_{GeSe}(r)$, the first peak at $\simeq$2.35 Å originates from Ge-Se heteropolar bonds, and gives a coordination number $\bar{n}_{GeSe}$ = 4.0 that is also insensitive to the model. For the case of $g_{GeGe}(r)$, there is no feature at $\simeq$2.4 Å (Ref. 13) for any of the models, and hence no evidence for Ge-Ge homopolar bonds. Each model is therefore consistent with the presence of Se_n chains that are linked by $Ge(Se_4)_{1/2}$ tetrahedra, where Ge and Se both satisfy the '8-N' rule. Within the framework of this rule, there are two simple models for the network structure of disordered Ge_xSe_{1-x} systems.[13] In the chemically ordered network (CON) model, Ge-Se bonds are favored such that only Ge-Se and Ge-Ge bonds are allowed for compositions with $x > 0.33$, whereas only Ge-Se and Se-Se bonds are allowed for compositions with $x < 0.33$. In the random covalent network (RCN) model there is a purely statistical distribution of bond types such that Se-Se bonds are allowed for $x > 0.33$ and Ge-Ge bonds are allowed for $x < 0.33$. In the RCN model, $\bar{n}_{GeGe}$ = 0.73 for the $GeSe_9$ composition and, for an N = 260 system, this corresponds to $N_{Ge-Ge} = \bar{n}_{GeGe} \times N_{Ge}/2 \simeq 10$ Ge-Ge homopolar bonds, where N_{Ge} = 26 is the number of Ge atoms in the system and the factor of two avoids double counting. As shown in Table II, the results for models I–IV are fully consistent with a chemically ordered network.

Of the partial pair-distribution functions, $g_{GeGe}(r)$ changes most between models I–IV. (Fig. 5) It is, therefore, the most sensitive of these functions to the size of the model and the temporal trajectory chosen for its production. In each of the $g_{GeGe}(r)$ functions, the first peak at $\sim$3 Å arises from Ge-Ge distances within the four-fold rings formed by ES $Ge(Se_4)_{1/2}$ tetrahedra, and the second peak at $\sim$3.6 Å arises from Ge-Ge distances between CS $Ge(Se_4)_{1/2}$ tetrahedra. As compared to model I, there is a significant reduction in height of the ES peak in $g_{GeGe}(r)$ for models II–IV, indicating a marked reduction in the fraction of these motifs. In addition, the CS peak for model II shows a bimodal distribution that is absent for models III and IV. The origin of this feature will be discussed in Sec. V C where the bond-angle distributions are considered. Overall, of the N = 260 systems, model III exhibits the largest statistical noise, which stems from the shortened time for relaxation of the glass structure at T = 300 K. In comparison, models II and IV were both prepared by using much longer relaxation times for the glass structure at T = 300 K, and in the case of model IV a more extended procedure was also used for quenching from the melt. The appearance of a bimodal peak in the model II $g_{GeGe}(r)$ function may therefore originate from the occurrence of incomplete structural relaxation during the quench schedule at temperatures higher than T = 300 K.

The Ge atoms in the network structure of $GeSe_9$ can be distinguished as according to whether they are involved in no four-fold rings Ge(0), one four-fold ring Ge(1), or two four-fold rings Ge(2).[57] In the absence of Ge-Ge homopolar bonds, these correspond to Ge atoms that are involved solely in CS $Ge(Se_4)_{1/2}$ tetrahedra (Ge(0)), or to Ge atoms that are involved in either one (Ge(1)) or two (Ge(2)) ES $Ge(Se_4)_{1/2}$ tetrahedra. The proportions of these Ge(ℓ) atoms (ℓ = 0, 1 or 2) for FPMD models I–IV are given in Table III, where a cutoff distance r_{cut} = 2.75 Å was used in the analysis. Model I gives a ratio ES/CS = 1, whereas an analysis with a larger cutoff distance r_{cut} = 2.9 Å gives a ratio ES/CS = 0.86 (Ref. 22). Both of these values are significantly greater than the ratio ES/CS = 0.08–0.18 found for models II–IV. In comparison, ratios of ES/CS = 0.19(3) or ES/CS = 0.31(6) are estimated from Raman and ^{77}Se magic angle spinning (MAS) nuclear magnetic resonance (NMR) spectroscopy experiments, respectively.[18,40]

Models II–IV were obtained for a larger system size than model I (N = 260 versus N = 120), and also correspond to independent temporal trajectories. Thus, the high proportion of ES configuration seen in model I (Ref. 22) is unlikely to be representative of the overall network structure for glassy $GeSe_9$. This observation is supported by the FPMD N = 400 atom model of Tafen and Drabold[36] that led to a $g_{GeGe}(r)$ function with small ES and large CS peaks, although the associated conformations are embedded within a highly defected network structure.

Table III: The proportions of Ge atoms involved in 0, 1 or 2 four-fold rings, as obtained from the FPMD models of glassy $GeSe_9$ by using a cutoff distance r_{cut} = 2.75 Å. Note that the same calculations were performed for model I in Ref. 22, but the values in that reference correspond to a larger cutoff distance r_{cut} = 2.9 Å.

Model	Ge(0)	Ge(1)	Ge(2)
I (Ref. 22)	50	50	0.0
II	92.3	7.7	0.0
III	84.7	15.3	0.0
IV	92.3	7.7	0.0

In order to rationalize the findings of model I for glassy $GeSe_9$ (Ref. 22), one could argue that it originates from a peculiar set of configurations that persisted during the quench from the liquid state. In this case, these configurations will have persisted in the liquid for a long time interval: Model I was obtained by selecting four independent starting configurations from the liquid-state temporal-trajectory, separated by

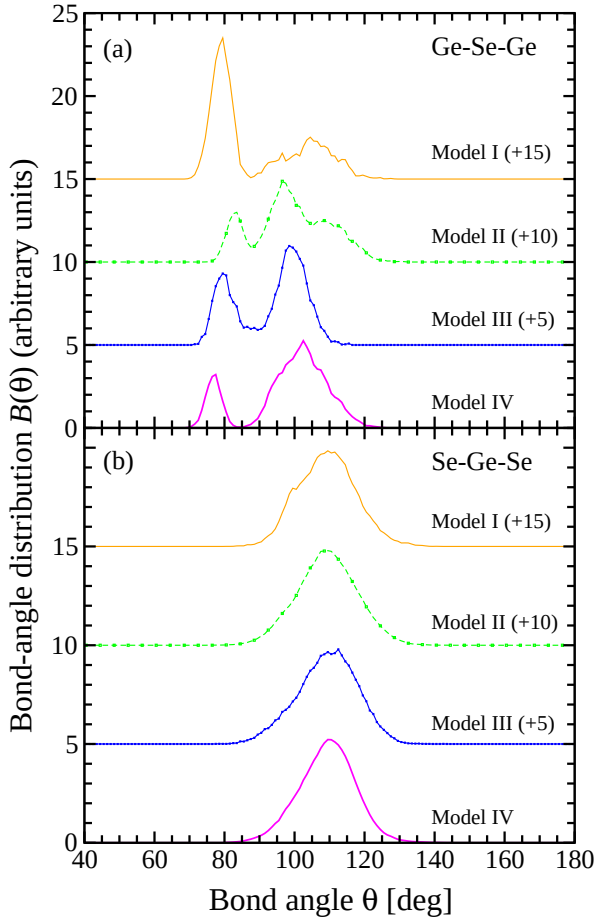

Figure 6: (Color online) The bond-angle distributions (a) $B(\theta_{\mathrm{GeSeGe}})$ and (b) $B(\theta_{\mathrm{SeGeSe}})$ for glassy $GeSe_9$, where a cutoff distance r_{cut} = 2.75 Å was used in the analysis. The results correspond to FPMD models I (solid orange curve),[22] II (broken green curve with squares), III (solid blue curve with squares) and IV (solid magenta curve). Several of the data sets have been shifted vertically for clarity of presentation.

time intervals of 5 ps, and quenching them to form a glass. It is therefore likely that the number of Ge atoms in model I (N = 120 with 12 Ge atoms) was simply too small to allow for a reliable statistical sampling of the possible Ge coordination environments on the timescale of the simulation.

C. Bond angle distributions

The Ge-Se-Ge bond-angle distributions $B(\theta_{\mathrm{GeSeGe}})$ for models I–IV of glassy $GeSe_9$ are shown in Fig. 6(a). All of these models give a peak at ∼80°, which originates from ES $Ge(Se_4)_{1/2}$ tetrahedra, and a feature at higher angles, which originates from CS $Ge(Se_4)_{1/2}$ tetrahedra. For the case of model I, there is a large fraction of ES motifs (Table III) and a correspondingly sharp ES peak in $B(\theta_{\mathrm{GeSeGe}})$. In comparison, the ES/CS ratio is smaller for models II–IV, and the ES feature in $B(\theta_{\mathrm{GeSeGe}})$ is less pronounced. For the case of model II, the CS feature in $B(\theta_{\mathrm{GeSeGe}})$ is split with a peak at ∼97° and a shoulder at ∼109°, where these items correspond in $g_{\mathrm{GeGe}}(r)$ to a peak at ∼3.5 Å and a shoulder at ∼3.8 Å, respectively (Fig. 5(a)). The type of CS conformations that are responsible for this peak splitting are shown in Fig. 7, where the five-fold ring shown in the left-hand panel contains a Se-Se homopolar bond. Five-fold rings were not, however, found in the networks of model IV, where a glass was formed from the liquid by adopting a longer temporal trajectory during the quench. The five-fold rings of model II may therefore be examples of the type of structural feature that appears only when the quench rate is particularly fast.

The Se-Ge-Se bond-angle distributions $B(\theta_{\mathrm{SeGeSe}})$ for models I–IV of glassy $GeSe_9$ are shown in Fig. 6(b). All of these models give a peak centered around 109°, which is indicative of CS $Ge(Se_4)_{1/2}$ tetrahedra. The $B(\theta_{\mathrm{SeGeSe}})$ for model I also has a shoulder at ∼99°, which corresponds to the smaller Se-Ge-Se angle found within ES conformations.

D. Structural units

One of the most intriguing questions regarding the structural organization in Ge_xSe_{1-x} glasses is the extent to which the Se_n chains are connected by $Ge(Se_4)_{1/2}$ tetrahedra. In this context, it is useful to consider the local coordination environment of two-fold coordinated Se atoms. Three different kinds of linkages are possible according to the chemical identity of the bonding atoms, namely Se-Se-Se, Ge-Se-Se and Ge-Se-Ge. It follows that, in the absence of Ge-Se-Se connections, the network will be phase separated into a Se-rich domain that is dominated by Se_n chains, and a $GeSe_2$-rich domain that is dominated by $Ge(Se_4)_{1/2}$ tetrahedra. This scenario has been proposed for glassy $GeSe_4$ on the basis of ^{77}Se NMR and Raman spectroscopy experiments,[12,17] but it is not substantiated by other experimental and theoretical work.[18,59–62] In order to describe the network connectivity for the different models of glassy $GeSe_9$, we consider the proportions of atoms of type α (α = Ge or Se) that are l-fold coordinated to other atoms $\bar{n}_\alpha(l)$, where the chemical identity of these other atoms needs to be specified. The proportions were calculated by finding, e.g., the number of Se atoms that are two-fold (l = 2) coordinated to one Ge and one Se atom, and dividing by the total number of Se atoms in the model. Bonds were deemed to be formed when the inter-atomic distance for a given pair of atoms is smaller than a cutoff distance r_{cut} = 2.75 Å, corresponding to the minimum after the first peak in $g_{\mathrm{T}}(r)$.

As shown by Table IV, none of the models for glassy $GeSe_9$ show any significant deviation from the coexistence of four-fold coordinated Ge atoms and two-fold coordinated Se atoms. The proportion of Se atoms in Se-Se-Se triads is in the 59–65% range, which compares to a value of 66(5)% from high-resolution isotropic ^{77}Se NMR spectra.[61] The proportion of Se atoms in Se-Se-Ge triads is, however, substantial at 26–35%, meaning that a significant number of the Se atoms are involved neither in Se_n chains nor in inter-tetrahedral Ge-Se-Ge connections. The proportion of Ge atoms in Ge-Se_4 linkages is predominant at ≥99.8%, emphasizing the chemically ordered nature of the glass network. The Ge-centered

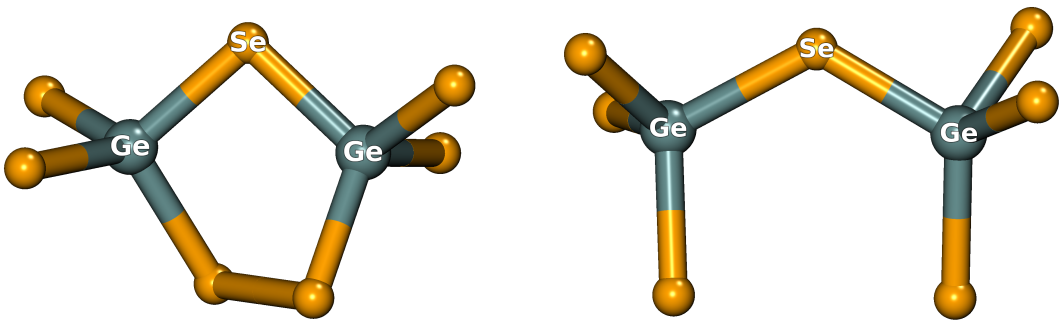

Figure 7: (Color online) The CS motifs in model II that lead to bi-modal CS features in both $g_{GeGe}(r)$ (Fig. 5(a)) and $B(\theta_{GeSeGe})$ (Fig. 6(a)). The Ge and Se atoms are represented by the dark (blue) and light (golden) balls, respectively, and the bonds are represented by sticks. Five-fold ring conformations of the type shown in the left-hand panel lead to peaks at ∼3.5 Å in $g_{GeGe}(r)$ and at ∼97° in $B(\theta_{GeSeGe})$. Conformations of the type shown in the right-hand panel lead to shoulders at ∼3.8 Å in $g_{GeGe}(r)$ and at ∼109° in $B(\theta_{GeSeGe})$.

Table IV: The proportions of the different structural units $\bar{n}_\alpha(l)$ in the FPMD models I–IV for glassy $GeSe_9$, as obtained by using a cutoff distance $r_{cut} = 2.75$ Å. The identity of the α atom (Ge or Se) at the center of a unit is given in bold font, and the identity of the l nearest neighbors is given in the second column. Note that the same calculations were also performed for model I in Ref. 22, but the values in that reference correspond to a larger cutoff distance $r_{cut} = 2.9$ Å.

		Proportion of $\bar{n}_\alpha(l)$ [%]			
		Model I	Model II	Model III	Model IV
Ge atom					
$l = 3$					
	Se_3	–	0.2	< 0.1	–
$l = 4$					
	Se_4	> 99.9	99.8	> 99.9	> 99.9
$l = 5$					
	$GeSe_4$	< 0.1	–	–	< 0.1
	Se_5	–	–	–	< 0.1
Se atom					
$l = 1$					
	Ge	–	0.4	0.8	< 0.1
	Se	0.2	1.1	0.8	< 0.1
$l = 2$					
	Se_2	64.6	58.9	59.0	60.1
	SeGe	25.9	33.5	33.8	35.0
	Ge_2	9.3	4.7	4.4	4.7
$l = 3$					
	Se_2Ge	< 0.1	1.2	0.3	< 0.1
	Se_3	0.1	0.2	0.5	< 0.1

tetrahedra are not, however, uniformly distributed on an intermediate length scale, as emphasized by the appearance of an FSDP in $S_{CC}(k)$ (Fig. 3).

VI. DISCUSSION OF THE SIMULATION PROTOCOLS

In the above, we have investigated the impact of three key variables in simulating the structure of glassy $GeSe_9$ by FPMD methods, namely (i) the system size, (ii) the quench schedule, and (iii) the final relaxation time at room temperature. This material has proved to be particularly challenging for FPMD simulations because of the small concentration of Ge atoms.

Focusing on the impact of the system size, the large number of ES units found for the $N = 120$ system of model I (Table III) turned out to be a byproduct of insufficient statistical sampling, which is associated with the limited number $N_{Ge} = 12$ of Ge atoms. A sizeable proportion of this small number of Ge atoms were trapped in unrepresentative configurations in the liquid that had little chance to evolve during the timescale of the simulation.

Turning to the impact of the quench schedule and structural relaxation at room temperature for the $N = 260$ systems, it is convenient to distinguish between "short" and "extended" temporal trajectories on the basis of a 10 ps threshold. Within this classification scheme, model III corresponds to short quench steps and a short relaxation time, is most affected by the statistical noise, and features the largest proportion of ES units (Table III). In comparison, model II corresponds to short quench steps and an extended relaxation time, and has a smaller proportion of ES units, i.e., the relaxation at room temperature appears to play an important role in affecting the glass structure. Lastly, model IV corresponds to extended quench steps and an extended relaxation time. Models II and IV differ by the occurrence of a bimodal distribution of CS units in model II (Fig. 7) that is not present in model IV, indicating the presence in model II of unstable configurations that are affected by the duration of the quench steps, and emphasizing the important role played by the quench schedule. Overall, our results illustrate the crucial roles played both by the quench schedule prior to relaxation at room temperature and by the relaxation process itself. The latter is likely to be an important issue when making plans for future work on amorphous structures by molecular dynamics models, which

are quite often constructed by considering the extent of the quench-schedule alone.

VII. CONCLUSIONS

The structure of glassy $GeSe_9$ was investigated by combining neutron diffraction with FPMD simulations, where three different models were prepared by using a periodic system containing $N = 260$ atoms and three independent temporal trajectories. The measured total structure factor is significantly different from that obtained in the previous neutron diffraction work of Ramesh Rao et al.,[39] and corresponds to a structure in which the overall mean coordination number $\bar{n}$ is in agreement with the '8-N' rule. The FPMD models lead to total structure factors and total pair-distribution functions that are in accord with the new experimental work. Each model gives a chemically ordered network in which $Ge(Se_4)_{1/2}$ tetrahedra interconnect Se_n chains, and the Ge and Se atoms are four-fold and two-fold coordinated, respectively. In contrast to previous FPMD results for glassy $GeSe_9$ performed on a system of $N = 120$ atoms,[22] the majority of $Ge(Se_4)_{1/2}$ tetrahedra are corner-sharing, with a ratio ES/CS = 0.08–0.18. The local coordination environment of Se does not point to any evidence of phase separation into Se-rich and $GeSe_2$-rich domains. A first-sharp diffraction peak in the Bhatia-Thornton concentration-concentration partial structure factor $S_{CC}(k)$ does, however, indicate a non-uniform distribution of the Ge-centered tetrahedra on an intermediate length-scale.

Acknowledgements

We thank Keiron Pizzey and Alex Hannon for help with the experimental work, and Mauro Boero and Guido Ori for valuable discussions. The Strasbourg group received support from GENCI for computer facilities (Allocations No. 2015095071 and No. 2015096092), and from the Direction Informatique (Pole HPC) of the University of Strasbourg through a generous allocation of computer time. Part of the HPC resource was funded by the Equipex Equip@Meso project. The support of the French/Korean international program of cooperation LIA-Nanofunc is also gratefully acknowledged. The Bath group received support from the EPSRC via Grants No. EP/G008795/1 and No. EP/J009741/1. AZ is supported by a Royal Society − EPSRC Dorothy Hodgkin Research Fellowship.

[1] R. Zallen, *The Physics of Amrophous Solids* (Wiley, New York, 1983).
[2] R. Azoulay, H. Thibierge, and A. Brenac, J. Non-Cryst. Solids **18**, 33 (1975).
[3] P. Tronc, M. Bensoussan, A. Brenac, and C. Sebenne, Phys. Rev. B **8**, 5947 (1973).
[4] W. Bresser, P. Boulchand, and P. Suranyi, Phys. Rev. Lett. **56**, 2493 (1986).
[5] A. Sugai, Phys. Rev. B **35**, 1345 (1987).
[6] I. T. Penfold and P. S. Salmon, Phys. Rev. Lett. **67**, 97 (1991).
[7] W. Zhou, M. Paesler, and D. E. Sayers, Phys. Rev. B **43**, 2315 (1991).
[8] P. S. Salmon and J. Liu, J. Phys.: Cond. Mat. **6**, 1449 (1994).
[9] X. Feng, W. J. Bresser, and P. Boolchand, Phys. Rev. Lett. **78**, 4422 (1997).
[10] Y. Wang, O. Matsuda, K. Inoue, O. Yamamuro, T. Matsuo, and K. Murase, J. Non-Cryst. Solids **232-234**, 702 (1998).
[11] I. Petri, P. S. Salmon, and H. E. Fischer, Phys. Rev. Lett. **84**, 2413 (2000).
[12] B. Bureau, J. Troles, M. Le Floch, P. Guénot, F. Smektala, and J. Lucas, J. Non-Cryst. Solids **319**, 145 (2003).
[13] P. S. Salmon, J. Non-Cryst. Solids. **353**, 2959 (2007).
[14] A. Sartbaeva, S. A. Wells, A. Huerta, and M. F. Thorpe, Phys. Rev. B **75**, 224204 (2007).
[15] M. T. M. Shatnawi, C. L. Farrow, P. Chen, P. Boolchand, A. Sartbaeva, M. F. Thorpe, and S. J. L. Billinge, Phys. Rev. B **77**, 094134 (2008).
[16] F. Inam, D. N. Tafen, G. Chen, and D. A. Drabold, Phys. Status Solidi B **246**, 1849 (2009).
[17] P. Lucas, E. A. King, O. Gulbiten, J. L. Yarger, E. Soignard, and B. Bureau, Phys. Rev. B **80**, 214114 (2009).
[18] E. L. Gjersing, S. Sen, and B. G. Aitken, J. Phys. Chem. C **114**, 8601 (2010).
[19] E. L. Gjersing, S. Sen, and R. E. Youngman, Phys. Rev. B **82**, 014203 (2010).
[20] S. Hosokawa, I. Oh, M. Sakurai, W.-C. Pilgrim, N. Boudet, J.-F. Bérar, and S. Kohara, Phys. Rev. B **84**, 014201 (2011).
[21] M. Bauchy, M. Micoulaut, M. Celino, S. Le Roux, M. Boero, and C. Massobrio, Phys. Rev. B **84**, 054201 (2011).
[22] M. Micoulaut, A. Kachmar, M. Bauchy, S. Le Roux, C. Massobrio, and M. Boero, Phys. Rev. B **88**, 054203 (2013).
[23] K. Wezka, A. Bouzid, K. J. Pizzey, P. S. Salmon, A. Zeidler, S. Klotz, H. E. Fischer, C. L. Bull, M. G. Tucker, M. Boero, et al., Phys. Rev. B **90**, 054206 (2014).
[24] A. Bouzid, K. J. Pizzey, A. Zeidler, G. Ori, M. Boero, C. Massobrio, S. Klotz, H. E. Fischer, C. L. Bull, and P. S. Salmon, Phys. Rev. B **93**, 014202 (2016).
[25] J. C. Phillips, J. Non-Cryst. Solids **34**, 153 (1979).
[26] M. F. Thorpe, J. Non-Cryst. Solids **57**, 355 (1983).
[27] P. Boolchand, D. G. Georgiev, and B. Goodman, J. Optoelectron. Adv. Mater. **3**, 703 (2001).
[28] P. Boolchand, X. Feng, and W. J. Bresser, J. Non-Cryst. Solids **293-295**, 348 (2001).
[29] S. Bhosle, K. Gunasekera, P. Chen, P. Boolchand, M. Micoulaut, and C. Massobrio, Solid State Commun. **151**, 1851 (2011).
[30] C. Massobrio, F. H. M. van Roon, A. Pasquarello, and S. W. De Leeuw, J. Phys.: Cond. Mat. **12**, L697 (2000).
[31] L. Giacomazzi, C. Massobrio, and A. Pasquarello, Phys. Rev. B **75**, 174207 (2007).
[32] S. Le Roux, A. Zeidler, P. S. Salmon, M. Boero, M. Micoulaut, and C. Massobrio, Phys. Rev. B **84**, 134203 (2011).
[33] K. Sykina, E. Furet, B. Bureau, S. Le Roux, and C. Massobrio, Chem. Phys. Lett. **547**, 30 (2012).
[34] S. Le Roux, A. Bouzid, M. Boero, and C. Massobrio, Phys. Rev. B **86**, 224201 (2012).
[35] S. Le Roux, A. Bouzid, M. Boero, and C. Massobrio, J. Chem.

Phys. **138**, 174505 (2013).
[36] D. N. Tafen and D. A. Drabold, Phys. Rev. B **71**, 054206 (2005).
[37] C. Massobrio, M. Celino, P. S. Salmon, R. A. Martin, M. Micoulaut, and A. Pasquarello, Phys. Rev. B **79**, 174201 (2009).
[38] A. Bouzid, S. Le Roux, G. Ori, M. Boero, and C. Massobrio, J. Chem. Phys. **143**, 034504 (2015).
[39] N. Ramesh Rao, P. S. R. Krishna, S. Basu, B. A. Dasannacharya, K. S. Sangunni, and E. S. R. Gopal, J. Non-Cryst. Solids. **240**, 221 (1998).
[40] S. Bhosle, K. Gunasekera, P. Boolchand, and M. Micoulaut, Int. J. Appl. Glass Science **3**, 205 (2012).
[41] A. C. Hannon, Nucl. Instrum. Methods Phys. Res. A **551**, 88 (2005).
[42] J. F. Jal, C. Mathieu, P. Chieux, and J. Dupuy, Phil. Mag. B **62**, 351 (1990).
[43] *http://www.isis.stfc.ac.uk/instruments/sandals/data-analysis/gudrun8864.html*.
[44] R. Car and M. Parrinello, Phys. Rev. Lett. **55**, 2471 (1985).
[45] A. D. Becke, Phys. Rev. A **38**, 3098 (1988).
[46] C. Lee, W. Yang, and R. G. Parr, Phys. Rev. B **37**, 785 (1988).
[47] M. Micoulaut, R. Vuilleumier, and C. Massobrio, Phys. Rev. B **79**, 214205 (2009).
[48] M. Micoulaut and C. Massobrio, J. Optoelect. Adv. Mat. **11**, 1907 (2009).
[49] C. Massobrio, M. Micoulaut, and P. S. Salmon, Solid State Sciences **12**, 199 (2010).
[50] N. Troullier and J. L. Martins, Phys. Rev. B **43**, 1993 (1991).
[51] H. E. Fischer, A. C. Barnes, and P. S. Salmon, Rev. Prog. Phys. **69**, 233 (2006).
[52] V. F. Sears, Neutron News **3**, 26 (1992).
[53] A. B. Bhatia and D. E. Thornton, Phys. Rev. B **2**, 3004 (1970).
[54] P. S. Salmon, Proc. Roy. Soc. London A **437**, 591 (1992).
[55] P. S. Salmon, S. Xin, and H. E. Fischer, Phys. Rev. B **58**, 6115 (1998).
[56] P. S. Salmon, Proc. Roy. Soc. London A **445**, 351 (1994).
[57] C. Massobrio and A. Pasquarello, Phys. Rev. B **75**, 014206 (2007).
[58] C. Massobrio, A. Pasquarello, and R. Car, Phys. Rev. B **64**, 144205 (2001).
[59] M. Kibalchenko, J. R. Yates, C. Massobrio, and A. Pasquarello, Phys. Rev. B **82**, 020202(R) (2010).
[60] M. Kibalchenko, J. R. Yates, C. Massobrio, and A. Pasquarello, J. Phys. Chem. C **115**, 7755 (2011).
[61] D. C. Kaseman, I. Hung, Z. Gan, and S. Sen, J. Phys. Chem. B **117**, 949 (2013).
[62] K. Sykina, B. Bureau, L. Le Pollès, C. Roiland, M. Deschamps, C. J. Pickard, and E. Furet, Phys. Chem. Chem. Phys. **16**, 17975 (2014).